Published in final edited form as:
Arch Ophthalmol. 2008 April ; 126(4): 537–542. doi:10.1001/archopht.126.4.537.

Imaging the Ocular Anterior Segment With Real-Time, Full-Range Fourier-Domain Optical Coherence Tomography

Marinko V. Sarunic, PhD, **Sanjay Asrani, MD**, and **Joseph A. Izatt, PhD**
Department of Biomedical Engineering (Drs Sarunic and Izatt), and the Duke Eye Center (Dr Asrani), Duke University, Durham, North Carolina

Abstract

We have demonstrated a novel Fourier-domain optical coherence tomography system and signal-processing algorithm for full-range, real-time, artifact-free quantitative imaging of the anterior chamber. Cross-sectional full-range images comprising 1024×800 pixels (axial×lateral) were acquired and displayed at 6.7 images/s. Volumetric data comprising 1024×400×60 pixels (axial×lateral×elevation) were acquired in 4.5 seconds with real-time visualization of individual slices and 3-dimensional reconstruction performed in postprocessing. Details of the cornea, limbus, iris, anterior lens capsule, trabecular meshwork, and Schlemm's canal were visualized. Quantitative surface height maps of the corneal epithelium and endothelium were obtained from the volumetric data and used to generate corneal thickness maps.

Currently, ophthalmology can benefit from detailed imaging of the ocular anterior segment for a variety of applications. Precise measurement of the dimensions and profiles of the interior structures of the anterior chamber are relevant for imaging abnormalities in the cornea, sclera, iris, and anterior chamber angle. Visualization of the trabecular meshwork and Schlemm's canal could be a valuable tool for glaucoma diagnosis and treatment and requires resolution in the range of tens of microns. Refractive surgeries, such as laser in situ keratomileusis and photorefractive keratectomy, would also benefit from accurate corneal mapping, especially if it could be performed noninvasively without compromising surgical-field sterility.

Several techniques are currently available for imaging the anterior segment of the eye, each suited to a specialized application. High-frequency ultrasound biomicroscopy provides resolution of up to 20 μm with a depth penetration of up to 5 mm in tissue at up to 8 frames/s, allowing in vivo imaging of the anterior chamber angle.[1,2] Ultrasound biomicroscopy requires immersion of the eye in a water bath with the patient in a supine position and is incompatible with concurrent slitlamp observation and high-volume patient screening. Ultrasonic pachymetry is regularly used for corneal thickness measurement but is a point-by-point technique. Automated scanning slit-based technologies, such as OrbScan (Bausch & Lomb, Rochester, New York), optically measure corneal topography and thickness,[3,4] which are required for refractive procedures, such as laser in situ keratomileusis and refractive power calculation for intraocular lens (IOL) implantations. The OrbScan, however, does not image

Correspondence: Joseph A. Izatt, PhD, Department of Biomedical Engineering, Duke University, 136 Hudson Hall, Durham, NC 27708 (jizatt@duke.edu)..

Additional Contributions: We thank Kevin Hsu, PhD, at Micron Optics Inc for loaning us the swept-source OCT, and Brian E. Applegate, PhD, and Robert J. Zawadzki, PhD, for their insightful discussions.

Financial Disclosure: Drs Sarunic and Izatt are inventors of intellectual property, assigned to Duke University, related to the subject of this article. Dr Izatt is a founder and part-time employee of Bioptigen Inc.

structures internal to the cornea or perform measurements of anterior chamber width, required, in addition to the depth, for the sizing and evaluation of phakic IOLs.

Optical coherence tomography (OCT) is an emerging technique for noninvasive cross-sectional imaging of biological tissue.[5] Time-domain OCT systems have been commercialized for retinal imaging (400-Hz, A-scan rate, Stratus OCT; Carl Zeiss Meditec, Dublin, California) and for ocular anterior segment imaging (2-kHz, A-scan rate, Visante; Carl Zeiss Meditec). In contrast to retinal OCT systems that operate at 830 nm,[6] anterior segment systems operate at 1310 nm owing to decreased attenuation in highly scattering tissues, such as the sclera.[7]

In recent years, OCT technology has been revolutionized by the development of Fourier-domain techniques,[8] which provide a significantly increased signal-to-noise ratio and increased robustness compared with traditional time-domain OCT.[9-11] The signal-to-noise ratio advantage of Fourier-domain OCT techniques may be employed for faster image acquisition, enabling practical 3-dimensional OCT imaging in patients for the first time. Two specific implementations of Fourier-domain OCT have been developed: spectrometer-based, or spectral-domain, OCT and swept-source OCT.[8] The increased sensitivity of both Fourier-domain OCT system designs comes at the price of limited usable imaging depth,[12] partially owing to the presence of a symmetric overlapping image artifact in Fourier-domain OCT images (Figure 1A). This artifact, referred to in the literature as the complex conjugate or mirror image artifact, occurs whenever the sample imaging depth spans both positive and negative distances compared with the length of the set reference path in the Fourier-domain OCT interferometer.

For retinal imaging at 830 nm, practical high-speed Fourier-domain OCT systems have been demonstrated with A-scan rates up to 30 kHz but with maximum imaging depths limited to approximately 2 mm.[13-17] Because healthy retinas are thinner than this, the complex conjugate artifact may be avoided by carefully positioning the patient's retina to keep it completely on one side of the reference position.

Fourier-domain OCT system designs at 1310 nm have been demonstrated with both spectral-domain OCT and swept-source OCT implementations, providing up to 20 kHz (spectral-domain OCT)[18] and 15.7 kHz[19] or 232 kHz[20] (swept-source OCT) A-scan rates. However, all 1310-nm Fourier-domain OCT systems operating at higher than a few kilohertz A-scan rate have been limited in maximum imaging depths to no deeper than 3 to 4 mm. In contrast to retinal imaging, full-depth imaging of the anterior chamber cannot be accommodated by the single-sided sample depth of previously demonstrated Fourier-domain OCT systems. Thus, a solution for the complex conjugate artifact is a prerequisite for bringing the advantages of the Fourier-domain OCT approach to anterior segment imaging.

Techniques borrowed from phase-shift interferometry have been demonstrated to suppress the complex conjugate artifact in Fourier-domain OCT, resolving positive and negative distances for low-speed, full-range imaging of the ocular anterior segment.[21-24] These techniques experienced image corruption from miscalibrated phase steps and sample motion, since they depended on sequential acquisition of phase-separated spectral interferograms. A polarization-encoding technique that simultaneously acquired two 90°-phase stepped interferograms has been presented in the literature[25] but was subject to corruption from birefringence. Instantaneous frequency-shifting techniques for full-range imaging have also been presented,[26-28] but are not compatible with spectrometer-based spectral-domain OCT systems.

We have recently described a novel approach using interferometers constructed from 3×3 optical couplers for simultaneous acquisition of phase-separated spectral interferometric data[29,30] as well as a high-speed compatible quadrature projection algorithm to correct for imperfect or miscalibrated phase shifts, including non-90°-phase shifts.[31] In this article, we

present a pilot study of the combination of these technologies to provide high-resolution, quantitative imaging of the ocular anterior segment in vivo using a quadrature projection 3×3 swept-source OCT system at an A-scan rate more than 3 times higher than that attainable with time-domain OCT systems.[7,32-34]

METHODS

This study was approved by the institutional review board of Duke University Medical Center. Six healthy volunteers underwent imaging with the novel Fourier-domain OCT system. The 3×3 Fourier-domain OCT system (Figure 2) was integrated into a standard slitlamp biomicroscope to assist in patient alignment, which required only a few seconds. A rapidly tunable laser source (Micron Optics Inc, Atlanta, Georgia) having a central wavelength of 1310 nm and an 84-nm full-width at half-maximum spectral width (corresponding to an OCT axial resolution of 9 μm in air) provided a sweep rate of 6.7 kHz. The mean optical power at the eye was 3.75 mW, which is well below the American National Standards Institute limit for maximum permissible exposure of 15.4 mW at this wavelength.[36] The lateral image resolution, defined as the full-width at half-maximum of the sample arm beam focus at the cornea, was 19 μm.

Full-range complex conjugate-resolved axial scans were generated by processing the 3 phase-separated detector outputs using the quadrature projection algorithm, described in detail elsewhere.[31] The full-range images were acquired, processed, and displayed in real time using custom software (modified from a base package provided by Bioptigen Inc, Durham, North Carolina) on a standard desktop computer. Each A-scan consisted of 1024 pixels. High-resolution images consisted of 800 A-scans and were displayed at 6.7 frames/s, and high-speed images consisted of 400 A-scans and were displayed at 13.4 frames/s. The volumes presented here consisted of 60 image elevations acquired in 4.5 seconds. During volume acquisition, “fly-through” images were displayed in real time. Volume rendering was performed in postprocessing using public-domain software (RMR Systems, Suffolk, England). The 3-dimensional images of the volumetric data appeared visually smooth and did not require additional processing for image registration owing to eye motion.

As described in previous reports of anterior segment imaging using time-domain OCT,[7,33,34,37] image processing was required to correct for light refraction at the air-cornea interface. To obtain quantitative corneal thickness measurements, we used a method for refraction correction based on Snell’s law (Figure 3).[38] The corneal epithelium and endothelium were manually segmented and fit by a fourth-order polynomial. The vertical difference between these lines represented the optical distance through the cornea, $d_{opt}(x)$. The angle at which the beam was refracted at the epithelium was calculated using the slope, $m_{epi}(x)$, given by the first derivative of the polynomial fit to the epithelial surface. Assuming a telecentric scan, the angle of incidence relative to the surface normal was given by $\theta_i=\tan^{-1}(m_{epi}[x])$. The angle of the refracted beam was given by $\theta_r=\sin^{-1}(\sin\theta_i/n_c)$, in which $n_c=1.38$, the assumed mean refractive index of the cornea.[39] The true location of the endothelial surface was calculated relative to the epithelial coordinates (x_{epi}, z_{epi}) using the relations $x_{cor}=x_{epi}-([d_{opt}/n_c]\sin\theta_r)$ and $z_{cor}=z_{epi}-([d_{opt}/n_c]\cos\theta_r)$. The corneal thickness was measured perpendicular to the slope of the epithelium at each lateral location. The corneal thickness map and the topographic maps of the corneal epithelium and endothelium resulting from these processing steps were smoothed by a 2-dimensional low-pass image filter.

RESULTS

We compared a complex conjugate artifact-resolved Fourier-domain OCT image of the healthy ocular anterior segment using quadrature projection processing with an unprocessed image

(Figure 1). In the complex conjugate-resolved image, the corneal epithelium, iris, anterior lens capsule, and anterior chamber angle were clearly observed. A faint image of the ciliary body was also observed. The dim artifactual line at the vertical center of the image (corresponding to the 0 path-length position) was due to imperfect subtraction of the reference spectrum in image processing. Higher-resolution images of the angle region were obtained by reducing the lateral scan length while preserving the number of A-scans per image (Figure 4). The trabecular meshwork and Schlemm's canal were visible, but the outline of the ciliary body was only dimly observed as a result of signal loss due to scattering in the tissue.

Volumetric Fourier-domain OCT imaging of the anterior segment is demonstrated in Figure 5. Cross-sectional planes of the angle (Figure 6) were acquired with the scan length reduced to 7 mm. The iris, limbus, and a faint outline of the ciliary body are visible. The images consisting of 1024×400×60 pixels (axial×lateral×elevation) were cropped to 512 pixels axially for volume rendering.

Topographic maps of the cornea were generated by postprocessing the volume image of the anterior chamber, providing a grid of 24 000 depth measurements across the cornea. A surface height map of the corneal epithelium is shown in Figure 7A. The endothelial surface height map in Figure 7B was corrected for refraction as described previously. The corneal thickness map obtained using the prototype 3×3 swept-source OCT system was compared against data from a commercial Pentacam system (Oculus, Dudenhofen, Germany) acquired from an adult male volunteer with normal vision. The results are shown in Figure 8 with the color and lateral dimension scales for the 3×3 swept-source OCT data matched to the graphical report from the commercial Pentacam system. The minimum corneal thickness measured with the swept-source OCT system was 580 μm, comparable with the 575-μm measurement provided by the Pentacam system.

COMMENT

The full-range, high-speed Fourier-domain OCT system presented here facilitated ocular anterior chamber imaging owing to an increased A-scan rate and denser pixel sampling compared with previous time-domain OCT systems.[7,32-34] The prototypical Fourier-domain OCT system used in this study operated at an A-scan rate of 6.7 kHz, which was limited by the acquisition speed of the digitization electronics. The ocular anterior segment images consisted of 1024 axial points, nearly double that of earlier time-domain systems.[7] Because of the increased sensitivity of Fourier-domain OCT techniques, the optical exposure was maintained at 3.75 mW (compared with 4.9 mW used in recent studies[7,33]), despite the higher system speed.

Schlemm's canal is nominally 100 to 200 μm in diameter and was not easily observed using earlier time-domain systems.[7,33] The Fourier-domain OCT system provided improved visualization of Schlemm's canal and the trabecular meshwork (Figure 4).

The increased A-scan rate of the Fourier-domain OCT system also facilitated volume acquisition, which was demonstrated here for the first time in the entire anterior segment. Volume rendering of 3-dimensional anterior segment Fourier-domain OCT data (Figure 5) permits convenient assessment of the cornea, iris, and pupil. Interactive manipulation of volumetric images (Figure 6) is very similar to techniques well known in diagnostic radiology and could become important for pathologic diagnosis, for example, facilitating assessment of the extent of tumors on the iris or ciliary body.

The corneal surface maps (Figure 8) were generated from large data sets (24 000 voxels), providing improved precision compared with point-by-point pachymetry, potentially allowing reliable fitting of aberrations with higher order than sphere and cylinder. Accurate surface

topographical and thickness measurements of the cornea, particularly in a noncontact imaging modality, are potentially useful for surgical monitoring and post-operative measurements. The increased signal-to-noise ratio of Fourier-domain OCT may also facilitate thickness mapping of hazy corneas after refractive surgeries for which disagreement has been demonstrated between measurements acquired using ultrasonic pachymetry and OrbScan.[3,4] Calculation of required refractive power is also beneficial for phakic IOL implantations, as is measurement of chamber depth and width, particularly for iris-anchored IOLs.

CONCLUSIONS

We have presented a full-range, quadrature projection 3×3 swept-source Fourier-domain OCT system, providing high-resolution, real-time display of the ocular anterior segment. The system was used to quantitatively measure corneal thickness and it provided images of the angle region. The high axial resolution of the Fourier-domain OCT system and increased lateral sampling facilitated in vivo imaging of Schlemm's canal.

Acknowledgments

Funding/Support: This study was supported by grants EY013516 and EY017393 from the National Eye Institute. Dr Asrani is a recipient of the Career Development Award from Research to Prevent Blindness Inc, New York, New York.

Appendix

Eye on the Web

Small Primate, Big Eyes

Tarsiers, some of the world's smallest primates, have the largest eyes relative to body size among mammals (Figure).[2] Human eyes would have to be the size of apples to match tarsier eye proportions. Surprisingly, they are named for their extremely long feet and not for their enormous and fascinating eyes, which take up about half of the relatively tiny face. Each eye is larger than the animal's brain or its stomach. Tarsiers originate from the Philippines and nearby islands and are mostly active at night. However, they lack a reflective tapetum lucidum characteristic of most nocturnal animals so having very large eyes helps to maximize their sensitivity in low light. Unlike many other nocturnal animals who have slit-shaped pupils, tarsiers have humanlike round pupils that are able to constrict very effectively to about half a millimeter.[3] Their eyes have retinae with both rods and cones and a fovea, which is unusual for nocturnal animals. The large crystalline lens aids in dim light.[4] Tarsiers cannot rotate their huge eyes; instead, they are able to turn their heads nearly 360°.

You can see the tarsier in action in an amusing 1939 black-and-white movie describing scientists at Yale University School of Medicine studying one to "better understand the human eyes" and to help in "designing everyday things."[5]

Ilya Rozenbaum, MD

Christoph Faschinger, MD, PhD

Robert Ritch, MD, Section Editor

Figure.
Tarsier eyes.[1]

References

1. [Accessed August 25, 2007]. Smile! http://www.flickr.com/photos/kenilio/130110478/in/set-72157594529074712
2. Kubicek, C.; University of Michigan Museum of Zoology animal diversity. Tarsius syrichta. 1999 [Accessed August 25, 2007]. Web site. http://animaldiversity.ummz.umich.edu/site/accounts/information/Tarsius_syrichta.html. Published
3. Land MF. Visual optics: the shapes of pupils. Curr Biol 2006;16(5):R167–R168. [PubMed: 16527734]
4. Collins CE, Hendrickson A, Kaas JH. Overview of the visual system of Tarsius. Anat Rec A Discov Mol Cell Evol Biol 2005;287(1):1013–1025. [PubMed: 16200648]
5. 1939 [Accessed August 25, 2007]. Here's lookinghttp://www.archive.org/details/HeresLoo1939

REFERENCES

1. Pavlin CJ, Sherar MD, Foster FS. Subsurface ultrasound microscopic imaging of the intact eye. Ophthalmology 1990;97(2):244–250. [PubMed: 2326015]
2. Marchini G, Pagliarusco A, Toscano A, Tosi R, Brunelli C, Bonomi L. Ultrasound biomicroscopic and conventional ultrasonographic study of ocular dimensions in primary angle-closure glaucoma. Ophthalmology 1998;105(11):2091–2098. [PubMed: 9818611]
3. Fakhry MA, Artola A, Belda JI, Ayala MJ, Alio JL. Comparison of corneal pachymetry using ultrasound and Orbscan II. J Cataract Refract Surg 2002;28(2):248–252. [PubMed: 11821205]
4. Kawana K, Tokunaga T, Miyata K, Okamoto F, Kiuchi T, Oshika T. Comparison of corneal thickness measurements using Orbscan II, non-contact specular microscopy, and ultrasonic pachymetry in eyes after laser in situ keratomileusis. Br J Ophthalmol 2004;88(4):466–468. [PubMed: 15031156]
5. Huang D, Swanson EA, Lin CP, et al. Optical coherence tomography. Science 1991;254(5035):1178–1181. [PubMed: 1957169]
6. Hee MR, Izatt JA, Swanson EA, et al. Optical coherence tomography of the human retina. Arch Ophthalmol 1995;113(3):325–332. [PubMed: 7887846]
7. Radhakrishnan S, Rollins A, Roth J, Yazdanfar S, Izatt J. Real-time optical coherence tomography of the anterior segment. Arch Ophthalmol 2001;119(8):1179–1185. [PubMed: 11483086]

8. Fercher AF, Hitzenberger CK, Kamp G, Elzaiat SY. Measurement of intraocular distances by backscattering spectral interferometry. Opt Commun 1995;117(12):43–48.doi:10.1016/0030-4018(95)00119-S
9. Leitgeb R, Hitzenberger CK, Fercher AF. Performance of fourier domain vs. time domain optical coherence tomography. Opt Express 2003;11(8):889–894. [PubMed: 19461802]
10. de Boer JF, Cense B, Park BH, Pierce MC, Tearney GJ, Bouma BE. Improved signal-to-noise ratio in spectral-domain compared with time-domain optical coherence tomography. Opt Lett 2003;28(21):2067–2069. [PubMed: 14587817]
11. Choma MA, Sarunic MV, Yang C, Izatt JA. Sensitivity advantage of swept source and Fourier domain optical coherence tomography. Opt Express 2003;11(18):2183–2189. [PubMed: 19466106]
12. Dorrer C, Belabas N, Likforman JP, Joffre M. Spectral resolution and sampling issues in Fourier-transform spectral interferometry. J Opt Soc Am B 2000;17(10):1795–1802.
13. Cense B, Nassif N, Chen TC, et al. Ultrahigh-resolution high-speed retinal imaging using spectral-domain optical coherence tomography. Opt Express 2004;12(11):2435–2447. [PubMed: 19475080]
14. Wojtkowski M, Srinivasan VJ, Ko TH, Fujimoto JG, Kowalczyk A, Duker JS. Ultrahigh-resolution, high-speed, Fourier domain optical coherence tomography and methods for dispersion compensation. Opt Express 2004;12(11):2404–2422. [PubMed: 19475077]
15. Leitgeb RA, Drexler W, Unterhuber A, et al. Ultrahigh resolution Fourier domain optical coherence tomography. Opt Express 2004;12(10):2156–2165. [PubMed: 19475051]
16. Bower, BA.; Zhao, M.; Chu, A.; Zawadzki, RJ.; Sarunic, MV.; Izatt, JA. Rapid volumetric imaging of the human retina in vivo using a low-cost, Fourier domain optical coherence tomography system. In: Tuchin, VV.; Izatt, JA.; Fujimoto, JG., editors. Coherence Domain Optical Methods and Optical Coherence Tomography in Biomedicine IX. Vol. 5690. International Society for Optical Engineering; Bellingham, WA: 2005.
17. Jiao SL, Knighton R, Huang XR, Gregori G, Puliafito CA. Simultaneous acquisition of sectional and fundus ophthalmic images with spectral-domain optical coherence tomography. Opt Express 2005;13(2):444–452. [PubMed: 19488371]
18. Yun SH, Tearney GJ, Bouma BE, Park BH, de Boer JF. High-speed spectral-domain optical coherence tomography at 1.3 μm wavelength. Opt Express 2003;11(26):3598–3604. [PubMed: 19471496]
19. Yun SH, Tearney GJ, de Boer JF, Iftimia N, Bouma BE. High-speed optical frequency-domain imaging. Opt Express 2003;11(22):2953–2963. [PubMed: 19471415]
20. Huber R, Wojtkowski M, Fujimoto JG. Fourier domain mode locking (FDML): a new laser operating regime and applications for optical coherence tomography. Opt Express 2006;14:3225–3237. [PubMed: 19516464]
21. Wojtkowski M, Kowalczyk A, Leitgeb R, Fercher AF. Full range complex spectral optical coherence tomography technique in eye imaging. Opt Lett 2002;27(16):1415–1417. [PubMed: 18026464]
22. Götzinger E, Pircher M, Leitgeb RA, Hitzenberger CK. High speed full range complex spectral domain optical coherence tomography. Opt Express 2005;13(2):583–594. [PubMed: 19488388]
23. Targowski P, Gorczynska W, Szkulmowski M, Wojtkowski M, Kowalczyk A. Improved complex spectral domain OCT for in vivo eye imaging. Opt Commun 2005;249(13):357–362.doi:10.1016/j.optcom.2005.01.016
24. Bachmann AH, Leitgeb RA, Lasser T. Heterodyne Fourier domain optical coherence tomography for full range probing with high axial resolution. Opt Express 2006;14(4):1487–1496. [PubMed: 19503473]
25. Vakoc BJ, Yun SH, Tearney GJ, Bouma BE. Elimination of depth degeneracy in optical frequency-domain imaging through polarization-based optical demodulation. Opt Lett 2006;31(3):362–364. [PubMed: 16480209]
26. Yun SH, Tearney GJ, De Boer JF, Bouma BE. Removing the depth-degeneracy in optical frequency domain imaging with frequency shifting. Opt Express 2004;12(20):4822–4828. [PubMed: 19484034]
27. Zhang J, Nelson JS, Chen ZP. Removal of a mirror image and enhancement of the signal-to-noise ratio in Fourier-domain optical coherence tomography using an electro-optic phase modulator. Opt Lett 2005;30(2):147–149. [PubMed: 15675695]

28. Davis AM, Choma MA, Izatt JA. Heterodyne swept-source optical coherence tomography for complete complex conjugate ambiguity removal. J Biomed Opt 2005;10(6):064005. [PubMed: 16409070]
29. Choma MA, Yang CH, Izatt JA. Instantaneous quadrature low-coherence interferometry with 3 × 3 fiber-optic couplers. Opt Lett 2003;28(22):2162–2164. [PubMed: 14649928]
30. Sarunic MV, Choma MA, Yang C, Izatt JA. Instantaneous complex conjugate resolved spectral domain and swept-source OCT using 3×3 couplers. Opt Express 2005;13(13):957–967. [PubMed: 19494959]
31. Sarunic MV, Applegate BE, Izatt JA. Real time quadrature projection complex conjugate resolved Fourier domain optical coherence tomography. Opt Lett 2006;31(16):2426–2428. [PubMed: 16880844]
32. Izatt JA, Hee MR, Swanson EA, et al. Micrometer-scale resolution imaging of the anterior eye *in vivo* with optical coherence tomography. Arch Ophthalmol 1994;112(12):1584–1589. [PubMed: 7993214]
33. Radhakrishnan S, Goldsmith J, Huang D, et al. Comparison of optical coherence tomography and ultrasound biomicroscopy for detection of narrow anterior chamber angles. Arch Ophthalmol 2005;123(8):1053–1059. [PubMed: 16087837]
34. Goldsmith JA, Li Y, Chalita MR, et al. Anterior chamber width measurement by high speed optical coherence tomography. Ophthalmology 2005;112(2):238–244. [PubMed: 15691557]
35. Choma MA, Hsu K, Izatt JA. Swept source optical coherence tomography using an all-fiber 1300-nm ring laser source. J Biomed Opt 2005;10(4):44009. [PubMed: 16178643]
36. American National Standards Institute. American National Standard for Safe Use of Lasers. Laser Institute of America; Orlando, FL: 2000. p. 45-49.ANSI Z 136.1-2000
37. Westphal V, Rollins AM, Radhakrishnan S, Izatt JA. Correction of geometric and refractive image distortions in optical coherence tomography applying Fermat's principle. Opt Express 2002;10(9): 397–404. [PubMed: 19436373]
38. Zawadzki, RJ.; Leisser, C.; Leitgeb, R.; Pircher, M.; Fercher, AF. 3D ophthalmic OCT with a refraction correction algorithm. In: Drexler, W., editor. Coherence Domain Optical Methods and Optical Coherence Tomography in Biomedicine IX. Vol. 5140. International Society for Optical Engineering; Bellingham, WA: 2003. p. 20-27.
39. Lin RC, Shure MA, Rollins AM, Izatt JA, Huang D. Group index of the human cornea at 1.3-mu m wavelength obtained in vitro by optical coherence domain reflectometry. Opt Lett 2004;29(1):83–85. [PubMed: 14719668]

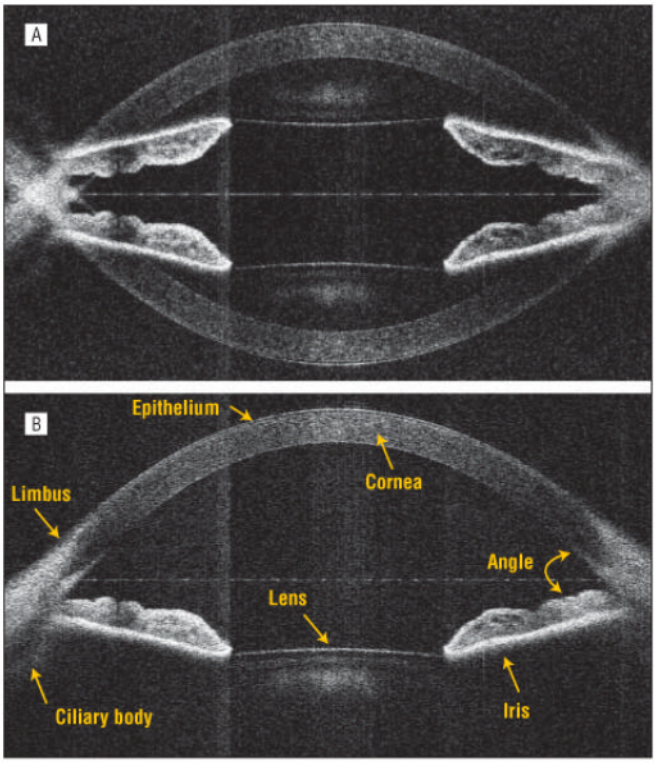

Figure 1.
Fourier-domain optical coherence tomography anterior segment images acquired in vivo on a human volunteer. A, Symmetric artifact between positive and negative distances observed in Fourier-domain optical coherence tomography systems. B, Quadrature projection processing of phase-stepped signals allows full-range imaging, uniquely resolving positive and negative distances. Each B-scan image, as shown previously, consists of 800 A-scans with 1024 pixels per A-scan, acquired and displayed in real time at 6.7 B-scans/s.

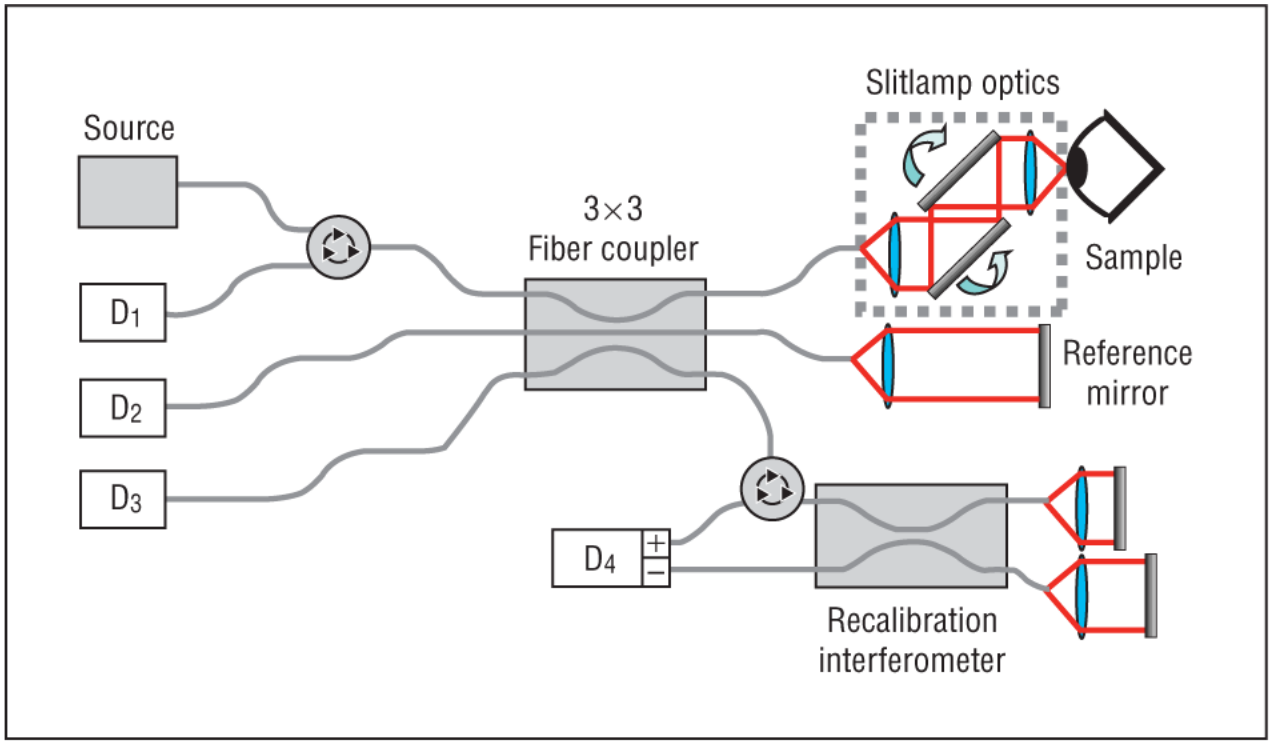

Figure 2.
Optical setup of the real-time full-range Fourier-domain optical coherence tomography system using a 3×3 fused fiber coupler in a Michelson type interferometer. The sample arm optics were integrated into a slitlamp biomicroscope to facilitate patient imaging. The separate 2×2 fiber-coupled Michelson interferometer was used to generate the wave number calibration signal.[35]

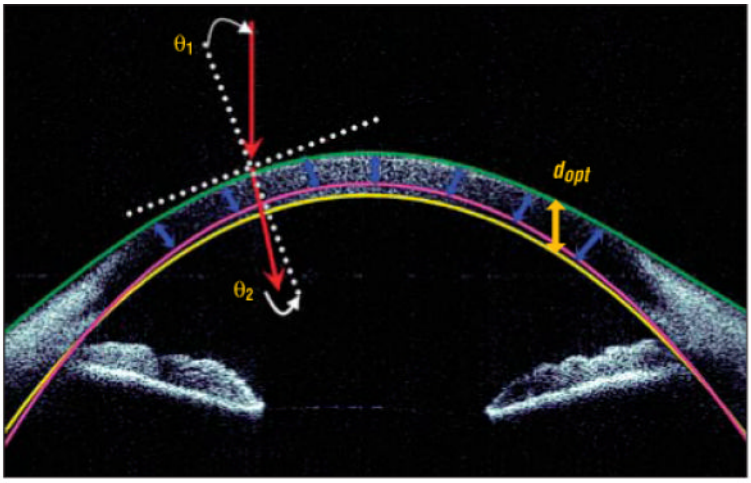

Figure 3.

Diagrammatic representation of the refraction correction procedure. The red arrow represents the Fourier-domain optical coherence tomography beam, incident on the cornea at angle θ_1 and refracted by angle θ_2. The orange arrow represents d_{opt}, the physical distance traveled by the beam through the cornea. The green and yellow lines represent the polynomial fits to the corneal epithelium and endothelium, respectively. The magenta curve represents the calculated actual location of the endothelial surface. Corneal thickness was measured perpendicular to the epithelium, as represented by the blue arrows.

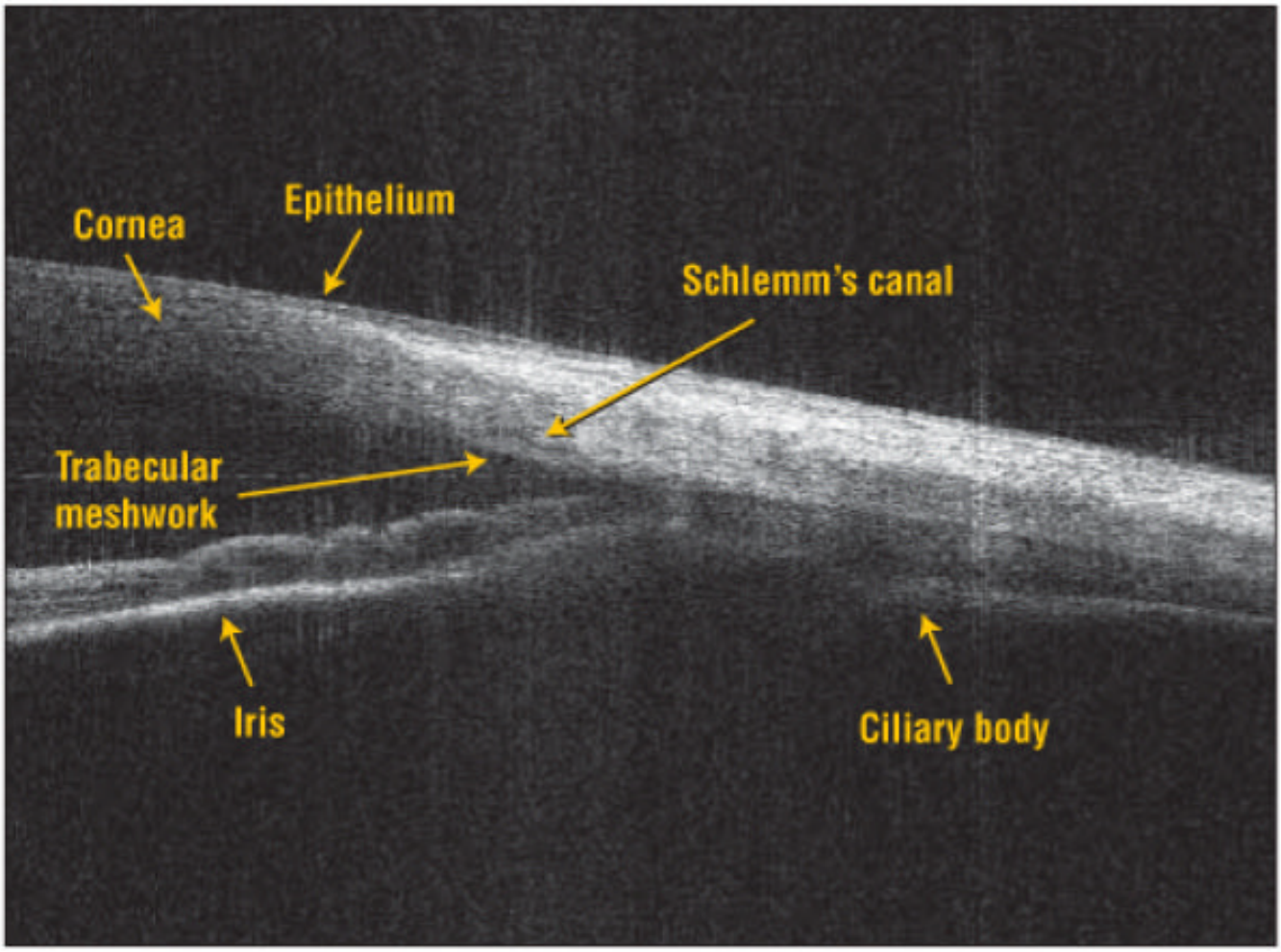

Figure 4.
High-resolution image of the anterior chamber angle. Clearly visible is the trabecular meshwork and Schlemm's canal. Visualization of the ciliary body appears improved compared with time-domain systems.

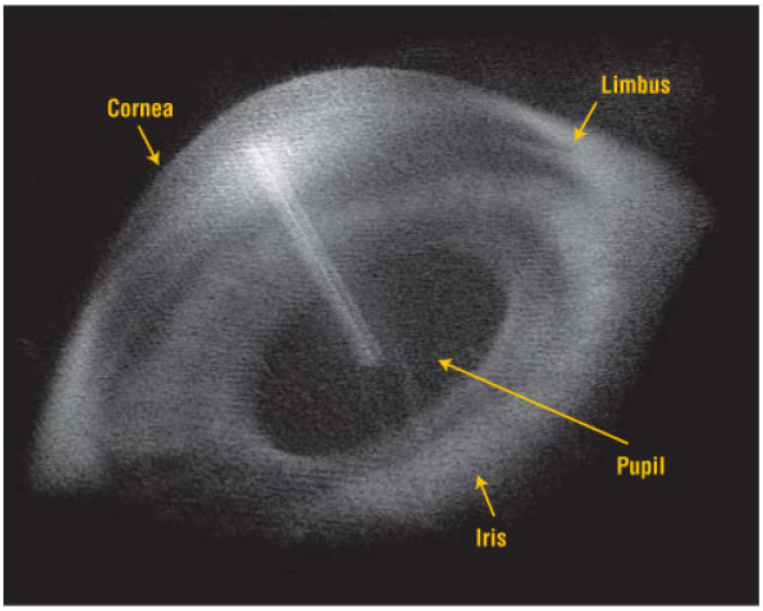

Figure 5.
Full-range volume reconstruction of the ocular anterior segment on a human volunteer.

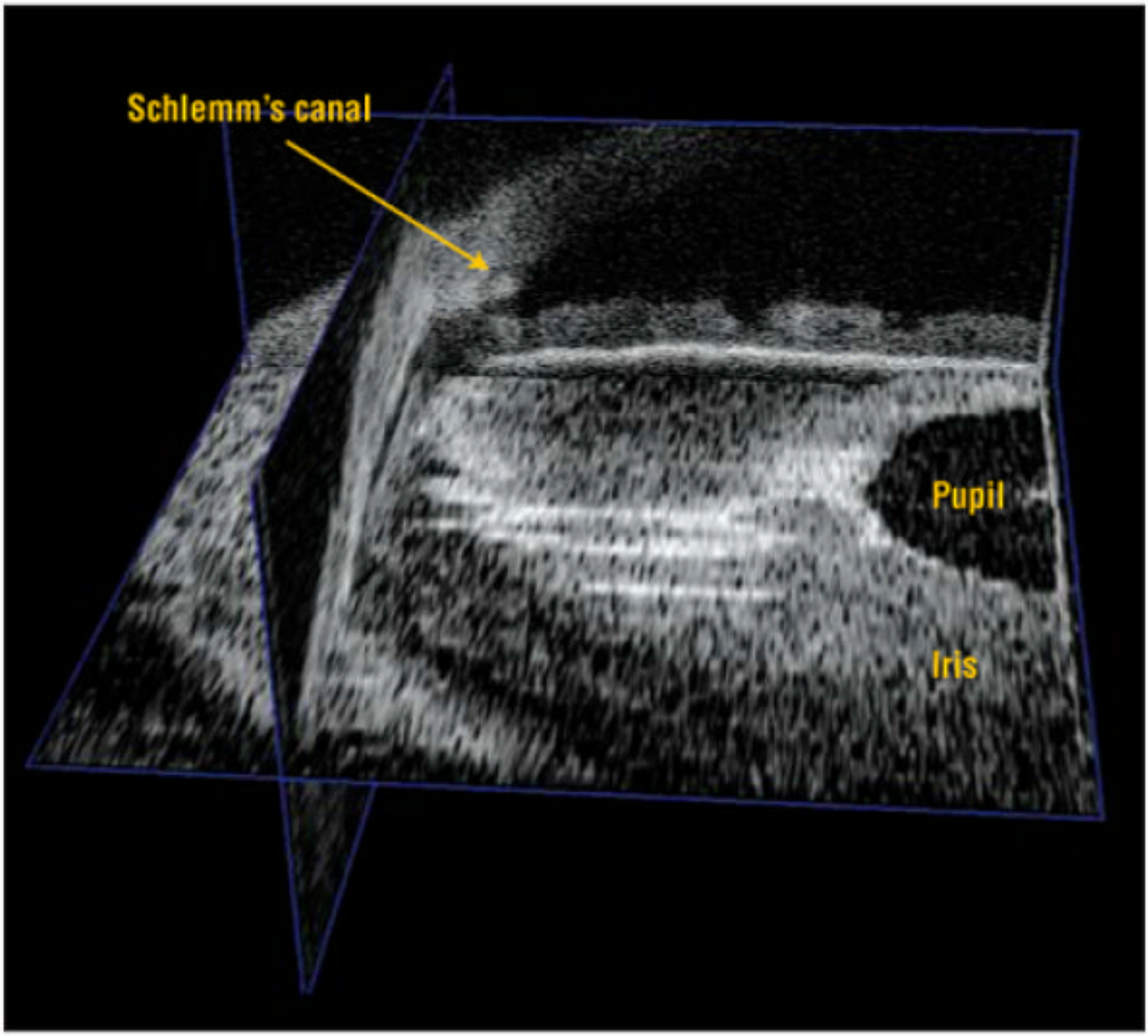

Figure 6.
Display of cross-sectional planes within a volume scan allows localization of structures. Three orthogonal planes (transverse, caudal, and sagittal) are shown through the volumetric reconstruction of the hemisphere of a human volunteer's ocular anterior chamber.

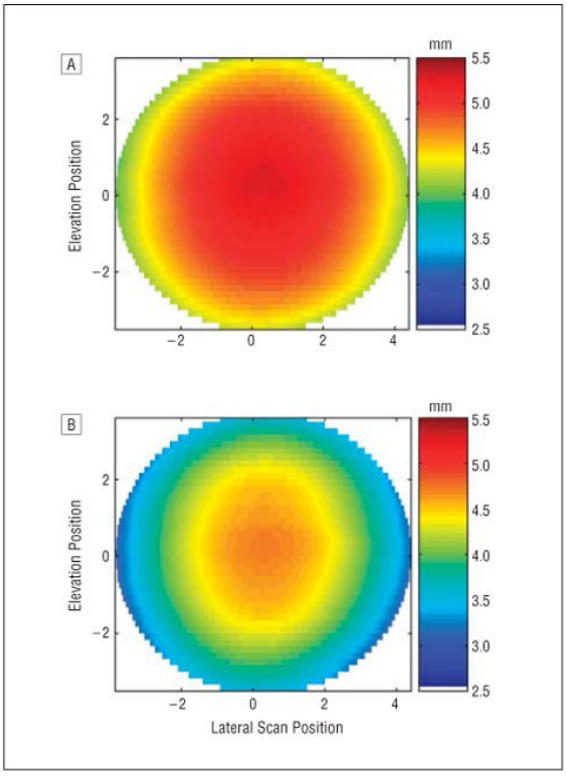

Figure 7.
Corneal topography measurements generated from the volumetric data presented in Figure 5. The epithelial height map (A) was extracted directly from the data, but the endothelial surface height map (B) required additional processing to correct for refraction.

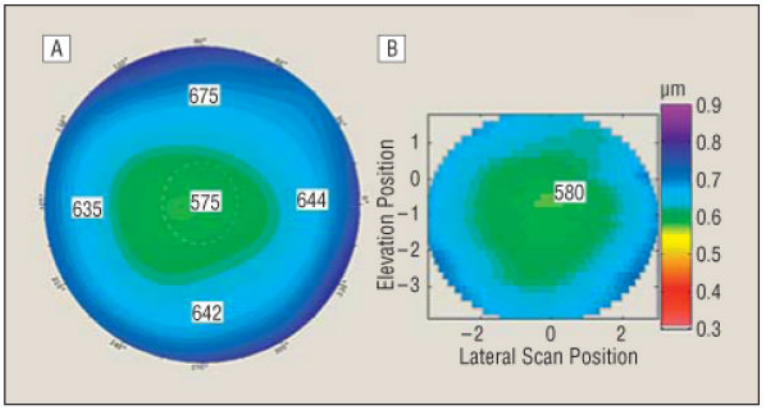

Figure 8.
Corneal thickness map comparison of a volunteer with normal vision generated using a commercial system (Pentacam; Oculus, Dudenhofen, Germany) (A) and the 3×3 swept-source optical coherence tomography prototype (B).